1. INTRODUCTION

Recently, there has been growing interest in underwater anthropogenic noise for environmental reasons. As a significant contribution to the underwater anthropogenic noise, shipping noise potentially poses a threat to marine fauna by damaging their hearing abilities and consequently interfering their behaviors including communication, feeding and prey. Driven by the motivation to prevent marine fauna from the adverse impact due to shipping noise, the produce of underwater noise maps has become the primary task which can guide the noise mitigation. This requires precise assessments of underwater radiated noise (URN) from vessels. The issue of URN measurements has been identified as one requiring further research, indicated by several recent collaborative projects, such as AQUQ (Achieve Quieter Oceans)[1][2] and SONIC (Suppression Of underwater Noise Induced by Cavitation)[3] launched by the EU (European Union).

For regulating the procedures of the URN measurements, the ISO (International standard organization) has issued the ISO 17208-1 standard,[4] in which three hydrophones placed at a distance of CPA (close point approach) from the ship are required to mitigate some aspects of water surface reflection, as shown in Figure. 1. The radiated noise level (RNL) at the hydrophones are converted to the source level (SL) by correcting the Lloyd's Mirror impact. One strong assumption made in the ISO 17208-1 standard is the flat water surface, which can be violated easily in practice. The water surfaces are randomly rough, or even time-dependent, in the real oceans, driven by wind forcing. Sound scattering from the rough water surfaces, therefore, affects the RNL at high frequencies (above 1 kHz), preventing the Lloyd's Mirror correction from being used directly.

The effects of sound scattering from rough water surfaces on URN measurements have been numerically investigated by Audoly and Meyer using the image model.[5] The roughness of the water surfaces was considered in the model by introducing a coherent reflection coefficient which reduces the effect of water surface reflection. The specular reflection, Hence, can be taken into account, while the component of scattering (incoherent field) representing the none-specular reflection is excluded. The absent incoherent field is vital for sound propagation at near-field on which the research of URN measurements focus. Further investigation should be undertaken to study the scattering effects on URN measurements with a model offering a full-wave solution of the wavefield.

This paper presents a numerical study of the effects of sound scattering from rough water surfaces on URN measurements. Two scenarios are considered including the deep water case with translationally symmetric surface waves and the shallow water case with two-dimensional rough surfaces. The deep and shallow water cases are simulated using an equivalent source method-based model[8] and a three-dimensional Helmholtz-Kirchhoff approximation, respectively, with the source-receiver configuration following the recommendation in the ISO 17208-1 standard as shown in Fig. 1. The remainder of this paper is organized as follows. Section.2 describes the modelling method before Section.3 presents numerical results and discussion. Finally, the conclusions to this study are summarized in Section. 4.

2. METHOD

A. UNDERWATER RADIATED NOISE MEASUREMENT MODEL

To simulate the URN measurements, the source-receiver configuration follows the recommendation of the ISO 17208-1 standard,[4] with the vessel modelled as a monopole point source placed at a depth of d_s, as shown in Fig. 1. Three hydrophones vertically immersed at a depth of d_{Hi} (i=1, 2 or 3) are placed at a CPA distance of d_{cpa} from the source. The measurement requires the vessel to transit along a given track, and to pass the hydrophone array at the CPA point. The data window (DW) shown in Figure. 2 (a) is the track truncated by two points at an angle of $\pm 30^\circ$ to the line linking the CPA point and hydrophone array.[4] The evaluation of the RNL of the vessel starts with the power average of the narrowband pressure across a

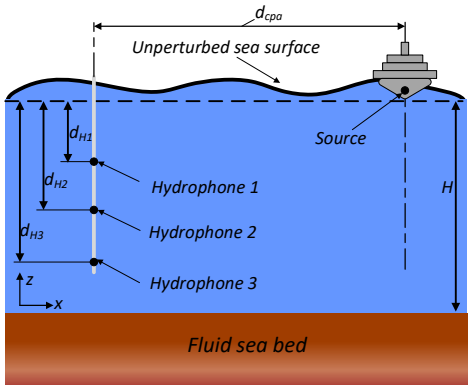

Figure 1: The hydrophone setup geometry for URN measurements in x-z plane.

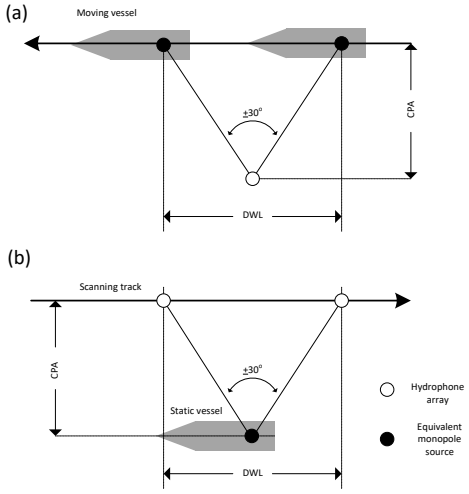

Figure 2: (a). The vessel manoeuver during trials and (b). The quasi-static model of the simulated trial.

series of sub-sections to which the DW is divided. Then, One-Third Octave (OTO) levels are obtained by integrating the narrowband results across each OTO band. Finally, the average across the three hydrohones gives the RNL of the vessel.

In this paper, the signal recorded by the hydrophone array when the source is moving is converted to the fields scanned by the hydrophone array at different spacial positions when the source is static as shown in Fig. 2 (b). Such a conversion is reasonable due to the negligible Doppler effects after performing the frequency average across OTO bands. The DW in the quasi-static model is defined as the scanning path extending $\pm 30^{\circ}$ either side of the CPA point about the source. For each run, the pressure field at the hydrophone array in the quasi-static model is calculated using either the ESM-based model or the 3D HKA that will be introduced in the next section. Here, multiple implementations of the wind-generated sea surfaces are required to study the scattering effects, and thus the ensemble average of the fields over the different implementations should be performed ahead of the average across the DW for individual runs. The evaluation of the RNL of the vessel can be formulated by:

$$RNL = RL + 20\log_{10}(\frac{d_{CPA}}{r_{ref}}), \tag{1}$$

where RL is the received level:

$$RL = 10\log_{10}(\frac{1}{3}\sum_{i}^{3}\frac{1}{N_f}\sum_{f}\frac{1}{N_\alpha}\sum_{\alpha} < |p_i(f,\alpha)|^2 >), \tag{2}$$

with $< \bullet >$, $\sum_f \bullet$ and $\sum_\alpha \bullet$ representing the ensemble average over different rough surface implementations, and the summation across DW sections OTO bands, respectively. Here, N_f and N_α are the numbers of frequency samples in each OTO band and sub-sections in the DW, and $p_i(f,\alpha)$ is the sound pressure received by i^{th} hydrophone at an angle of α to the line linking the CPA point and source at frequency f. Note that, the theoretical RNL of a point source is 0 dB, and thus the RNL calculated by Eq.(1) also represents the correction factor (CF) to compensate the real transmission loss for deducing the equivalent source level of the vessel.

B. ROUGH SEA SURFACE MODEL

A wind speed- and fetch length-dependent model, Joint North Sea Wave Project (JONSWAP)[6] spectra, is utilized to model the wind-generated surfaces. The 2-D surface is calculated by assuming azimuthal symmetry of the 1-D JONSWAP spectra about (k_x, k_y). Here, k_x and k_y are the 2-D wavenumber. Note that, the JONSWAP spectra in the wavenumber domain is converted from that in the frequency domain using the dispersion relation for shallow water[7] . After multiplying $S(k_x, k_y)$ by the cos-squared spreading factor $\cos^2(\theta)$ where θ is the phase angle of $k_x + ik_y$, the 2D surface height distribution is realized using the 2D Fourier transform. The default fetch length was set to be 10 km in this paper.

C. ACOUSTIC PROPAGATION MODEL

The 3-D pressure field $p_i(f,\alpha)$ is calculated using an ESM-based model for the deep water case with translationally symmetric surfaces and using the 3-D Helmholtz-Kirchhoff approximation (HKA) for the shallow water case with 2-D rough surfaces. Details about the ESM-based model will not be presented here for the effective use of the space, which can be seen in Ref.[8]

The derivation of the 3-D HKA is summerized here. The starting point is to consider the Helmholtz integral equation applied to the sound field below a pressure-release boundary,[9] with the scattered field given by:

$$p_s(\boldsymbol{r}_d, \boldsymbol{r}) = \int_\Gamma G(\boldsymbol{r}_\Gamma, \boldsymbol{r})\frac{\partial p(\boldsymbol{r}_d, \boldsymbol{r}_\Gamma)}{\partial n}d\Gamma, \tag{3}$$

where $G(\boldsymbol{r}_\Gamma, \boldsymbol{r})$ is the water/seabed half-space Green's function for the shallow water case. A complex image method[10] is used to calculated the Green's function. The complex image method is capable of handling the cases of the fluid seabed with two homogenous layers, and only few orders of complex images can provide a good accuracy.[10] In this paper, 5 order of complex images is used for the case of shallow water. $\frac{\partial p(\boldsymbol{r}_\Gamma, \boldsymbol{r})}{\partial n}$ is the normal derivative of the total pressure on the rough surface. In the Kirchhoff approximation, it follows:

$$\frac{\partial p(\boldsymbol{r}_d, \boldsymbol{r}_\Gamma)}{\partial n} \simeq 2\frac{\partial p_{inc}(\boldsymbol{r}_d, \boldsymbol{r}_\Gamma)}{\partial n}. \tag{4}$$

Here, the normal derivative of the incident field to the rough surface is given by:

$$\frac{\partial p_{inc}(\boldsymbol{r}_d, \boldsymbol{r}_\Gamma)}{\partial n} = \bigtriangledown p_{inc} \bullet \vec{\boldsymbol{n}}. \tag{5}$$

where $\vec{\boldsymbol{n}}$ is the normal of the rough surface:

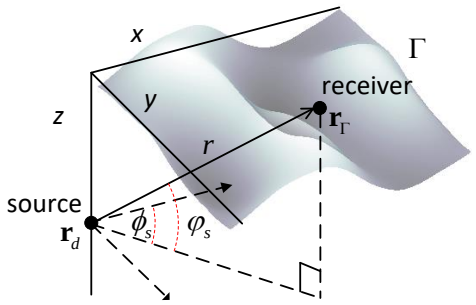

Figure 3: The scheme of the 3D Helmholtz-Kirchhoff approximation for a 2D surface.

$$\overrightarrow{\boldsymbol{n}} = \frac{(- \bigtriangledown \eta, 1)}{\sqrt{1 + (\bigtriangledown \eta)^2}}, \tag{6}$$

where η is the wave height function of x and y. The integral in Equation 3 then becomes:

$$\begin{aligned} p_s(\boldsymbol{r}_d, \boldsymbol{r}) =& 2 \iint w G_{3D}(\boldsymbol{r}_\Gamma, \boldsymbol{r}) (- \frac{\partial p_{inc}(\boldsymbol{r}_d, \boldsymbol{r}_\Gamma)}{\partial r} \frac{\partial \eta}{\partial x} \cos\psi_s \cos\phi_s \\ & - \frac{\partial p_{inc}(\boldsymbol{r}_d, \boldsymbol{r}_\Gamma)}{\partial r} \frac{\partial \eta}{\partial y} \cos\psi_s \sin\phi_s + \frac{\partial p_{inc}(\boldsymbol{r}_d, \boldsymbol{r}_\Gamma)}{\partial z}) dx dy, \end{aligned} \tag{7}$$

where $w = 1/\sqrt{1 + (\bigtriangledown \eta)^2}$, ϕ_s and ψ_s shown in Figure. 3 are the azimuth and elevation angle of the incident sound wave. To evaluate the integral in Eq.(7) numerically, the 2D rough sea surfaces are truncated at $x = \pm 125$ m and $y = \pm 125$ m with the point source as the origin. Even discretization of the surface is applied in both the x-axis and y-axis directions with 5 points per wavelength, guaranteeing the accuracy of the HKA.

3. NUMERICAL SIMULATION

A. SIMULATION PARAMETERS

For evaluating the correction factor (CF), OTO bans covering from 31.5 Hz to 10 kHz were considered with $N_f = 21$ per band, and the DW was divided into 13 sections with a α increment of 5° initially ($N_\alpha = 13$). The ensemble average evaluated the CF in the presence of wind-generated rough surfaces and associated uncertainties over 30 implementations of random rough sea surfaces. Simulations were carried out using the default environmental parameters and configuration shown in Table. 1.

B. RESULTS AND DISCUSSION

i. Deep water case

Figure. 4 displays the correction factors (CFs) of the total, coherent and incoherent fields for various wind speeds. The CFs of the total field show apparent dipole pattern below 100 Hz, with the fluctuation decreasing as the wind speed increases for the frequency ranging from 100 Hz to 2000 Hz. Above 2000 Hz, the CFs of the total field approach relatively constant around 3 dB. Such a constant depends on the source-receiver configuration and the CPA distance. For non-zero wind speed, the CFs of the coherent field gradually reduce to 0 dB as the frequency increases, decreasing more rapidly for stronger wind intensities. This is caused by the scattering effects intensified by the increase of roughness of the water surfaces due to the increased wind speed. Consequently, the coherent field representing the specular reflection is weakened,

Table 1: Environment Parameters and source-receiver configuration.

Parameter	Deep water	Shallow water
Source depth (m) d_s	4	4
Distance of CPA (m) D_{cpa}	100	100
Top hydrophone dpeth (m) d_{H1}	26.8	15
Middle hydrophone dpeth (m) d_{H2}	57.7	35
bottom hydrophone dpeth (m) d_{H3}	100	55
Water sound speed (m/s) c_1	1490	1490
Water density (kg/m^3) ρ_1	1000	1000
Seabed sound speed (m/s) c_2	/	1749
Seabed attenuation (dB/ λ) α_2	/	0.9
Seabed density (kg/m^3) ρ_2	/	1941

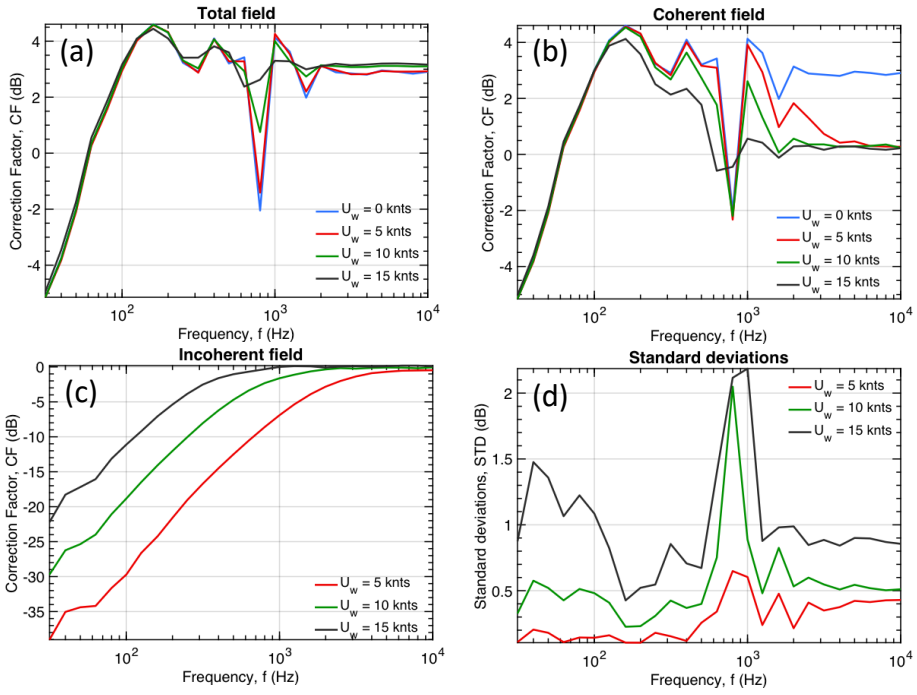

Figure 4: Correction factors of the (a) total, (b) coherent and (c) incoherent fields, and (d) the associated standard deviations, for wind speeds of 0 knots, 5 knots, 10 knots and 15 knots in deep water.

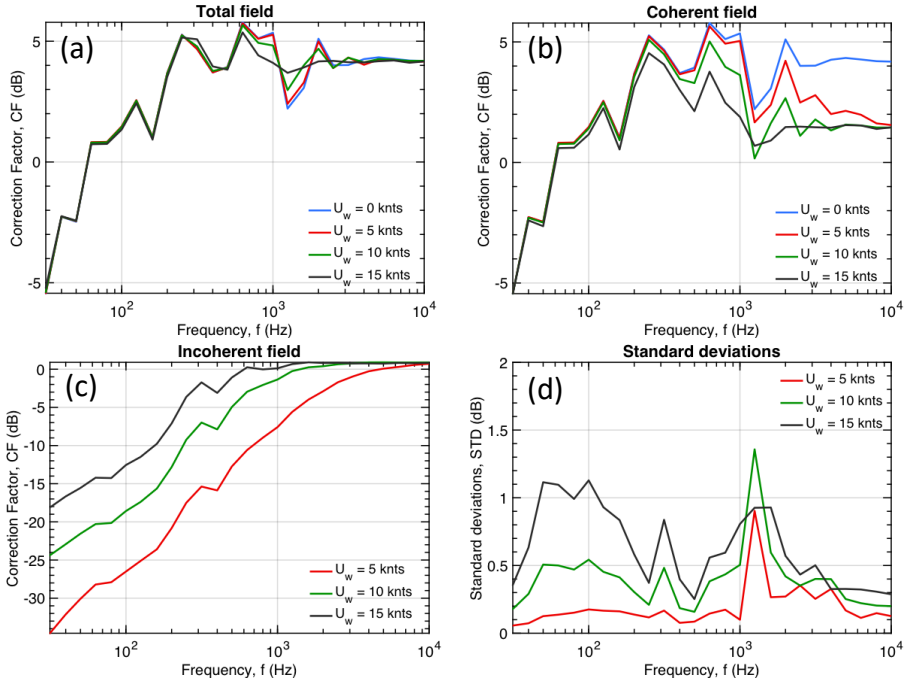

Figure 5: Correction factors of the (a) total, (b) coherent and (c) incoherent fields, and (d) the associated standard deviations, for wind speeds of 0 knots, 5 knots, 10 knots and 15 knots in shallow water.

which coincides with the reduction of the Lloyds mirror impact at higher frequencies demonstrated by Audoly.[5] On the contrary, the incoherent field representing the scattering component plotted in Fig. 4 (c) shows the opposite behaviour to the coherent field, tending to compensate the coherent loss at higher frequencies. The behaviour of the compensation from the incoherent field to the coherent loss explains why the CFs approach relatively constant at higher frequencies.

On the other hand, the STDs shown in Fig. 4 (d) exhibit an overall increase as the wind speed increases, pronouncing significant peaks at around 1000 Hz where the depths can be seen in the CFs of total and coherent fields. This indicates that the rise of the depths may only depend on the source-receiver configuration, which would be useful for minimizing the sensitivity of measurements by optimizing the source-receiver configuration.

ii. Shallow water case

Next, Figure. 5 gives the relevant results in shallow water with the parameters shown in Table. 1. In this case, the behaviors of the CFs of the total, coherent and incoherent are very similar to those in the deep water case. Note that, the constant, at which the CFs of the total field remain stable, increase 1 dB compared with the deep water case, depending on not only the source-receiver configuration and CPA distance but also parameters of the seabed.[12] Also, the peaks in the STDs reduce to no more than 1.5 dB in shallow water case, which indicates that the interference between the surface- and seabed-reflections may decrease the sensitivity of measurements.

4. CONCLUSION

This paper presents a numerical study of the effects of water surface roughness on the URN measurements. Both the deep water case with translationally symmetric surfaces and the shallow water case with 2-D rough surfaces have been demonstrated using an ESM-based model and the 3-D HKA, respectively. The results showed that, at higher frequencies, the coherent reflection coefficient reduces surface reflection and, hence, correction factor. Nevertheless, scattering becomes significant at higher frequencies. Including the scattered field component results in the correction factor being relatively constant at higher frequencies. The presented results ignore bubble scattering, which will potentially introduce attenuation as well as scattering and consequently affects the correction factor at higher frequencies.

REFERENCES

[1] Audoly, C *et al.*, "Mitigation of underwater radiated noise related to shipping and its impact on marine life: A practical approach developed in the scope of AQUO project", *IEEE Journal of Oceanic Engineering*. **42**(2), 373-387 (2017).

[2] Audoly, C and Rizzuto, E, "AQUO: Achieve quieter oceans by shipping noise footprint reduction fp7-collaborative project n 314227, wp 2: Noise sources, task t2. 1,"ship underwater radiated noise patterns"", (2015).

[3] Prins *et al.*, "Suppression of underwater noise induced by cavitation: SONIC", *Transportation Research Procedia.* **14**, 2668-2677 (2016).

[4] ISO, "Underwater acoustics — quantities and procedures for description and measurement of underwater sound from ships — part 1: Requirements for precision measurements in deep water used for comparison purposes", *ISO 17208-1, International Standardization Organization, Geneva, 2016*, (2016).

[5] Audoly, C and Meyer, V, "Measurement of radiated noise from surface ships-influence of the sea surface reflection coefficient on the lloyd's mirror effect", (2017).

[6] Hasselmann *et al.*, "Measurements of wind-wave growth and swell decay during the joint north sea wave project (JONSWAP)", *Ergänzungsheft.* , 8-12 (1973).

[7] Ballard, M. S, "Three-dimensional acoustic propagation under a rough sea surface", *Proceedings of Meetings on Acoustics ICA2013, Acoustical Society of America.* **Vol. 19, p.**, 070077 (2013).

[8] He *et al.*, "Three-dimensional sound scattering from transversely symmetric surface waves in deep and shallow water using the equivalent source method", *The Journal of the Acoustical Society of America.* **148**(1), 73-84 (2020).

[9] Thorsos, E. I, "The validity of the kirchhoff approximation for rough surface scattering using a gaussian roughness spectrum", *The Journal of the Acoustical Society of America.* **83**(1), 78-92 (1988).

[10] Fawcett, J. A, "Complex-image approximations to the half-space acousto-elastic green's function", *The Journal of the Acoustical Society of America.* **108**(6), 2791-2795 (2000).

[11] Brooker, A and Humphrey, V, "Measurement of radiated underwater noise from a small research vessel in shallow water", *Ocean Engineering.* **120**, 182-189 (2016).

[12] Meyer, V and Audoly, C, "A parametric study of the environment and the array configuration for underwater noise measurement from ships in shallow water", *Proceedings of the 26th International Congress on Sound and Vibration.* (2019).